Journal of Catalysis **195,** 193–206 (2000)
doi:10.1006/jcat.2000.2985, available online at http://www.idealibrary.com on IDEAL®

Effects of Pd Particle Size and Ceria Loading on NO Reduction with CO

Joseph H. Holles,* Robert J. Davis,*,[1] Thomas M. Murray,† and James M. Howe†

*Department of Chemical Engineering and †Department of Materials Science and Engineering, University of Virginia, Charlottesville, Virginia 22904-4741

Received April 21, 2000; revised June 28, 2000; accepted June 29, 2000

The kinetics of the NO + CO reaction from 433 to 573 K were studied over supported Pd with and without ceria promotion. In addition, temperature-programmed desorption (TPD) of products formed from preadsorbed NO was performed. For the ceria-promoted samples, the interface between Pd and ceria was changed by varying particle size and the amount of ceria postdeposited on the Pd particles. The Pd particle size affected both activity and apparent reaction orders. For the unpromoted catalyst, the Pd particle size of about 4.5-nm average diameter, determined by dihydrogen chemisorption, had a lower turnover frequency than 1-nm size particles, indicating structure sensitivity of the NO + CO reaction. However, the ceria-promoted samples showed a maximum in catalytic activity for 2-nm Pd. This maximum in reaction rate suggests a balance between the Pd/ceria interface which promotes NO dissociation and the Pd metal surface which catalyzes product formation. Results from TPD of adsorbed NO are consistent with this interpretation. High-resolution transmission electron microscopy was used to confirm the proximity of small ceria crystallites to the supported Pd particles. © 2000 Academic Press

Key Words: **NO; NO_x; CO; Pd (palladium); ceria; kinetics; reduction; NO + CO reaction; TPD; TEM; chemisorption.**

INTRODUCTION

Recently, there has been considerable interest in using palladium-only catalysts for automobile three-way exhaust gas conversion (1). Three-way converters (TWC) are designed to reduce emissions of carbon monoxide, nitrogen oxides, and uncombusted hydrocarbons. These catalysts typically contain noble metals such as Pt, Pd, and Rh with a ceria promoter supported on alumina. Traditionally, the principal function of the Rh is to control emissions of nitrogen oxides (NO_x) (1) by reaction with carbon monoxide. However, use of Pd to control NO_x emissions has increased. As a result, the NO + CO reaction has been studied on high surface area Pd/Al_2O_3 powder catalysts (2–6). Although ceria effectively promotes Rh for the NO + CO reaction (7), its use as a promoter for Pd has not been as widely studied (6, 8).

The NO + CO reaction was found to be structure sensitive over Pd single crystals with the Pd(111) facet being more active than either Pd(110) or Pd(100) (2, 9, 10). In addition, large particles (120 nm) of Pd supported on alumina were much more active than small particles (<3 nm) (2, 3). The Pd surface structure also affects dinitrogen selectivity for this reaction. The less active crystal faces tend to produce more N_2 and less N_2O (2). Furthermore, temperature-programmed desorption of adsorbed NO indicated that only N_2 desorbed from the small particles whereas both N_2 and N_2O desorbed from large particles (11). Interestingly, no appreciable particle size effect on dinitrogen selectivity was observed during the NO + CO reaction (2).

In our previous investigation of supported Pd for the NO + CO reaction, we showed that substantial improvements in reaction rates are realized when ceria is added as a promoter (6). This enhanced activity due to ceria addition is similar to that previously reported for Rh, which was attributed to new ceria–metal interfacial sites that promote NO dissociation (7). These results suggest that increasing the interfacial contact between Pd and ceria may further enhance catalytic activity for the NO + CO reaction.

Therefore, the present study examines the influence of Pd particle size and ceria loading on catalytic activity for the NO + CO reaction. Dihydrogen chemisorption, temperature-programmed desorption (TPD) of NO, and transmission electron microscopy were used to characterize the catalyst samples.

Typical three-way catalysts operate at temperatures around 900 K and do not exhibit appreciable NO_x reduction activity except in a narrow temperature window in the vicinity of catalyst light-off (1). This is a concern during cold start since the catalyst has not yet warmed up to operating temperature and a significant amount of total emissions are released during this period. Thus, the reaction temperatures used in this work are less than 573 K to simulate the state of the catalyst relevant to cold-start conditions.

[1] To whom correspondence should be addressed. Department of Chemical Engineering, Chemical Engineering Bldg. Rm. #117A, University of Virginia, 102 Engineers Way, Charlottesville, VA 22904-4741. Fax: (804) 982-2658. E-mail: rjd4f@virginia.edu.

0021-9517/00 $35.00
Copyright © 2000 by Academic Press
All rights of reproduction in any form reserved.

EXPERIMENTAL

The Pd/Al_2O_3 samples were prepared by slurrying γ-Al_2O_3 (Alfa Aesar, 99.97%) and palladium(II) acetylacetonate (acac) (Aldrich, 99%) in toluene for 2 h at 353 K and drying under vacuum in a rotary evaporator followed by 24 h in air at 473 K. Samples were then calcined in flowing air (BOC gases) by heating to 673 K at 0.5 K min^{-1} and then remaining at 673 K for 4 h. Subsequent reduction of the catalyst occurred at 673 K for 2 h in flowing dihydrogen (99.999% from BOC gases, passed through a Matheson Model 8371V purifier). For catalysts supported on CeO_x/Al_2O_3, the promoter was first deposited on the alumina by slurrying cerium(III) acetylacetonate hydrate (Aldrich) and alumina in toluene for 2 h at 353 K and then drying and calcining as described above. The palladium was then deposited on the CeO_x/Al_2O_3 using the same procedure used for the alumina-supported samples. Samples with CeO_x on Pd/Al_2O_3 had 1 wt% palladium deposited and reduced prior to addition of ceria. After incorporation of the promoter, the catalyst was calcined and reduced again.

The reaction experiments were performed in a quartz, single-pass, fixed bed reactor containing approximately 50 mg of catalyst diluted in chromatographic silica gel (Fisher). Feed gases included 5.00%NO/5.07%CO/He and He (99.999%) from BOC Gases, CO (UHP) from Air Products, and NO (99%) from MG Industries. Gas flow rates were controlled using mass flow controllers (Brooks Series 5850C) and varied from 5 to 250 ml min^{-1}. Total pressure in the reactor was atmospheric with partial pressures of the reactants varied by changing the individual flow rates while simultaneously adjusting the flow rate of pure He. Reactant and product analyses involved a combination of gas chromatography (HP 5890 Series II with an Alltech CTR I column) and mass spectrometry (Dycor MA 100 model). The standard catalyst pretreatment consisted of heating at 523 K for 1 h under flowing He. Product analysis was performed after a period of 45 min on stream at each set of reaction conditions to allow the reaction to reach steady state. Arrhenius-type plots were determined using 5.07 kPa of each NO and CO for the NO + CO reaction. For the determination of reaction orders, the partial pressure of NO or CO was held constant at 4.05 kPa while the pressure of the other gas was varied from 1.01 to 16.2 kPa.

TPD experiments were performed in an atmospheric pressure flow system with a quadrupole mass spectrometer (Dycor MA 100 model). A fresh catalyst sample of 1 g was heated in He (99.999% from BOC Gases) at 773 K for 3 h. The sample was then cooled to 303 K and then exposed to 10 ml min^{-1} NO (99% from MG Industries) in 10 ml min^{-1} He for 0.25 h. The system was then purged with He at 303 K for 2 h to remove weakly adsorbed NO. The temperature of the sample was increased linearly by 5 K min^{-1} to promote desorption of products into a He carrier stream (20 ml min^{-1}). The gas phase concentrations of N_2 (mass 28), NO (mass 30), O_2 (mass 32), and N_2O (mass 44) were monitored throughout the temperature ramp with the mass spectrometer. The amount of each gas desorbed was quantified by comparing the area under the TPD curve to peak areas of N_2, NO, and O_2 (99.993% BOC Gases) and N_2O (99.97%, BOC gases) calibration pulses injected after each experiment. The calibration pulses were also used to determine the contribution of N_2O cracking to mass 30 (NO) and mass 28 (N_2).

The percent of the Pd metal atoms exposed was determined using H_2 chemisorption (99.999% from BOC Gases passed through a Supelco OMI purifier) in a Coulter Omnisorp 100CX system. Sample pretreatment consisted of reduction in flowing H_2 at 663 K for 30 min followed by evacuation (10^{-5} mbar) at 673 K for 45 min to remove sorbed hydrogen (surface and bulk). Adsorption isotherms were obtained at 303 K. The hydrogen uptake was calculated from the difference between total chemisorption and reversible chemisorption. Elemental analysis was performed by Galbraith Laboratories Inc., Knoxville, TN and by Southern Testing and Research Laboratories Inc., Wilson, NC.

Samples were prepared for transmission electron microscopy (TEM) by placing the catalyst in ethanol and sonicating for 0.5 to 1 h to disperse the sample. One drop of solution was then placed on lacey carbon supported on a 300-mesh copper grid (Ted Pella, Inc.). The samples were then dried in air and stored in a desiccator. The micrograph images of the catalyst samples were acquired using a JEOL 4000 EX model transmission electron microscope at 400 kV, achieving a maximum magnification of 600,000×.

RESULTS

Results from elemental analysis are presented in Table 1. The $Pd/CeO_x/Al_2O_3$ samples had palladium deposited after the ceria whereas the $CeO_x/Pd/Al_2O_3$ samples had ceria deposited after the palladium. For the samples with ceria deposited first, the loading of cerium was on the order of that needed for a theoretical monolayer (~9 wt% Ce, based on the Ce surface density of 4.83 Ce/nm^2 derived from the CeO_2(110) plane). Very small and broad X-ray diffraction peaks associated with CeO_2 indicated that the promoter was well dispersed on the alumina.

Results from H_2 chemisorption on the supported metals are included in Table 1. Representative dihydrogen adsorption isotherms for 5 wt% Pd/Al_2O_3, 1 wt% Pd/Al_2O_3, and 0.5 wt% Pd/Al_2O_3 are presented in Figs. 1a–1c. Adsorption isotherms for the ceria-promoted samples are similar. The isotherms for two of the samples exhibited a large uptake of dihydrogen at about 3 kPa due to the formation of a β-phase hydride which is stable at 303 K at pressures greater than 2.3 kPa (12). The isotherms for the 0.5 wt% Pd/Al_2O_3 did not show the large uptake associated with β-hydride

TABLE 1

Elemental Analyses and Chemisorption Results

Catalyst	wt% Metal[a]	wt% Cerium[a]	H/M[b]	Particle size (nm)
0.5 wt% Pd/Al_2O_3	0.51	—	0.79	1.1
1 wt% Pd/Al_2O_3	0.96	—	0.59	1.5
5 wt% Pd/Al_2O_3	4.92	—	0.18	4.5
CeO_x/Al_2O_3	—	10.83	—	—
1 wt% $Pd/CeO_x/Al_2O_3$	0.87	8.66	1	<1
5 wt% $Pd/CeO_x/Al_2O_3$	4.12	10.66	0.46	2.0
10 wt% $Pd/CeO_x/Al_2O_3$	10.2	7.03	0.10	9.0
5 wt% $CeO_x/Pd/Al_2O_3$	0.70	4.89	0.29	3.1
10 wt% $CeO_x/Pd/Al_2O_3$	0.76	10.2	0.29[c]	3.1
30 wt% $CeO_x/Pd/Al_2O_3$	0.60	28.0	0.29[c]	3.1

[a] Quantitative analysis by Galbraith Laboratories Inc. and Southern Testing and Research Laboratories Inc.

[b] Total chemisorption-reversible chemisorption at 303 K.

[c] Based on value for 5 wt% $CeO_x/Pd/Al_2O_3$ sample.

formation in Pd particles. This result indicates that the Pd particles in this sample were too small to have significant internal volume to form the β-phase hydride. Average particle sizes for the samples, determined using $d = 0.9$/fraction metal exposed (13), are also shown in Table 1. Dihydrogen spillover from the Pd to the ceria resulted in the measured dispersion of the postdeposited ceria samples being unrealistically high, and therefore, the dispersion was assumed equal to the 5 wt% $CeO_x/Pd/Al_2O_3$ sample.

Transmission electron micrographs are shown in Fig. 2 for γ-Al_2O_3, 10 wt% CeO_x/Al_2O_3, 5 wt% $CeO_x/Pd/Al_2O_3$, and 30 wt% $CeO_x/Pd/Al_2O_3$. A comparison of Fig. 2b to Fig. 2a reveals that small ceria crystallites of about 3-nm average size are dispersed over the alumina support. Figure 2c shows a large Pd particle (~20 nm) with a small ceria crystallite about 5 nm deposited on it. Finally, Fig. 2d shows a slightly larger size Pd particle with numerous ceria crystallites of 3 to 7 nm deposited around it.

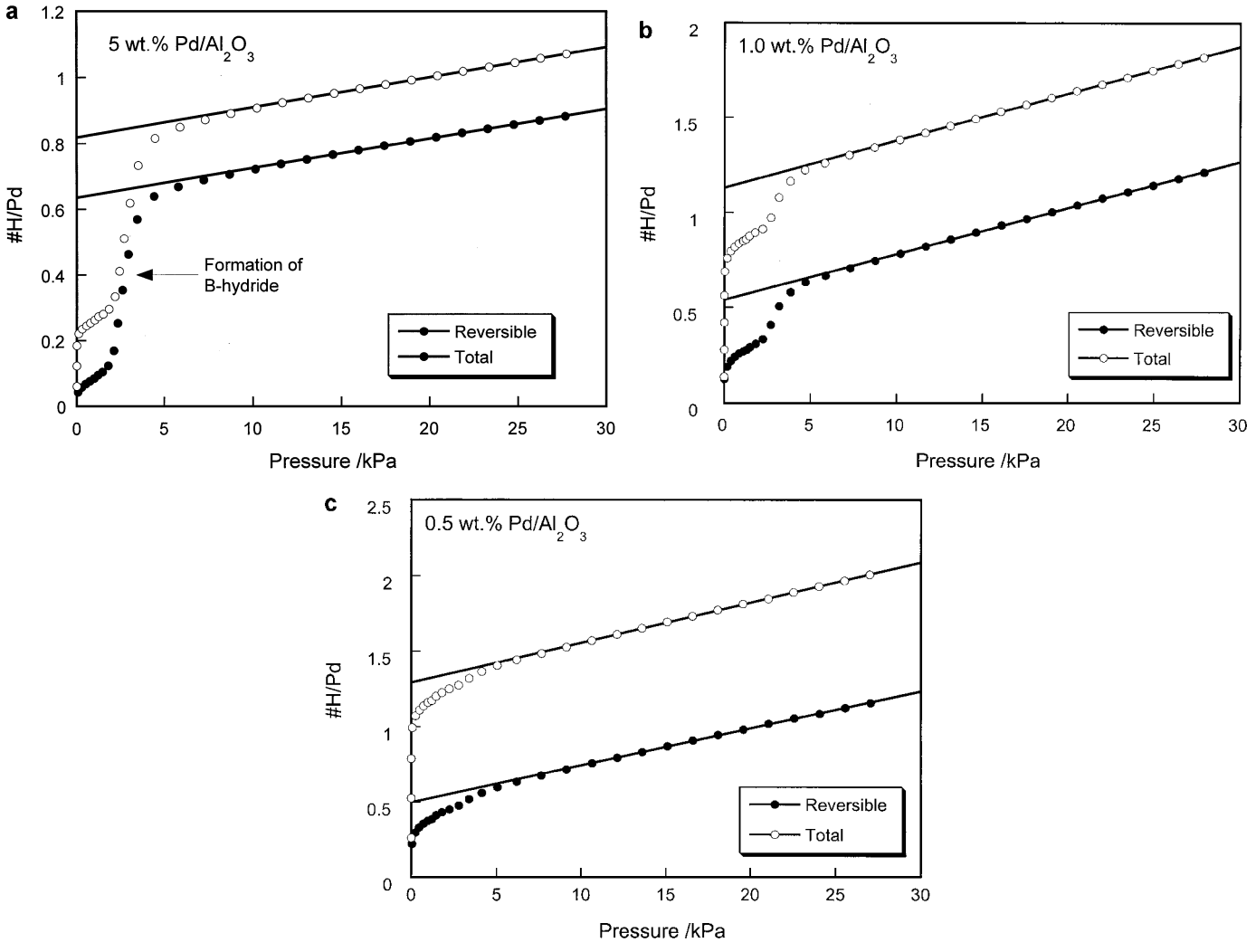

FIG. 1. Dihydrogen chemisorption isotherms for (a) 5 wt% Pd/Al_2O_3, (b) 1.0 wt% Pd/Al_2O_3, and (c) 0.5 wt% Pd/Al_2O_3. Lines indicate extrapolated values of total and reversible dihydrogen uptake.

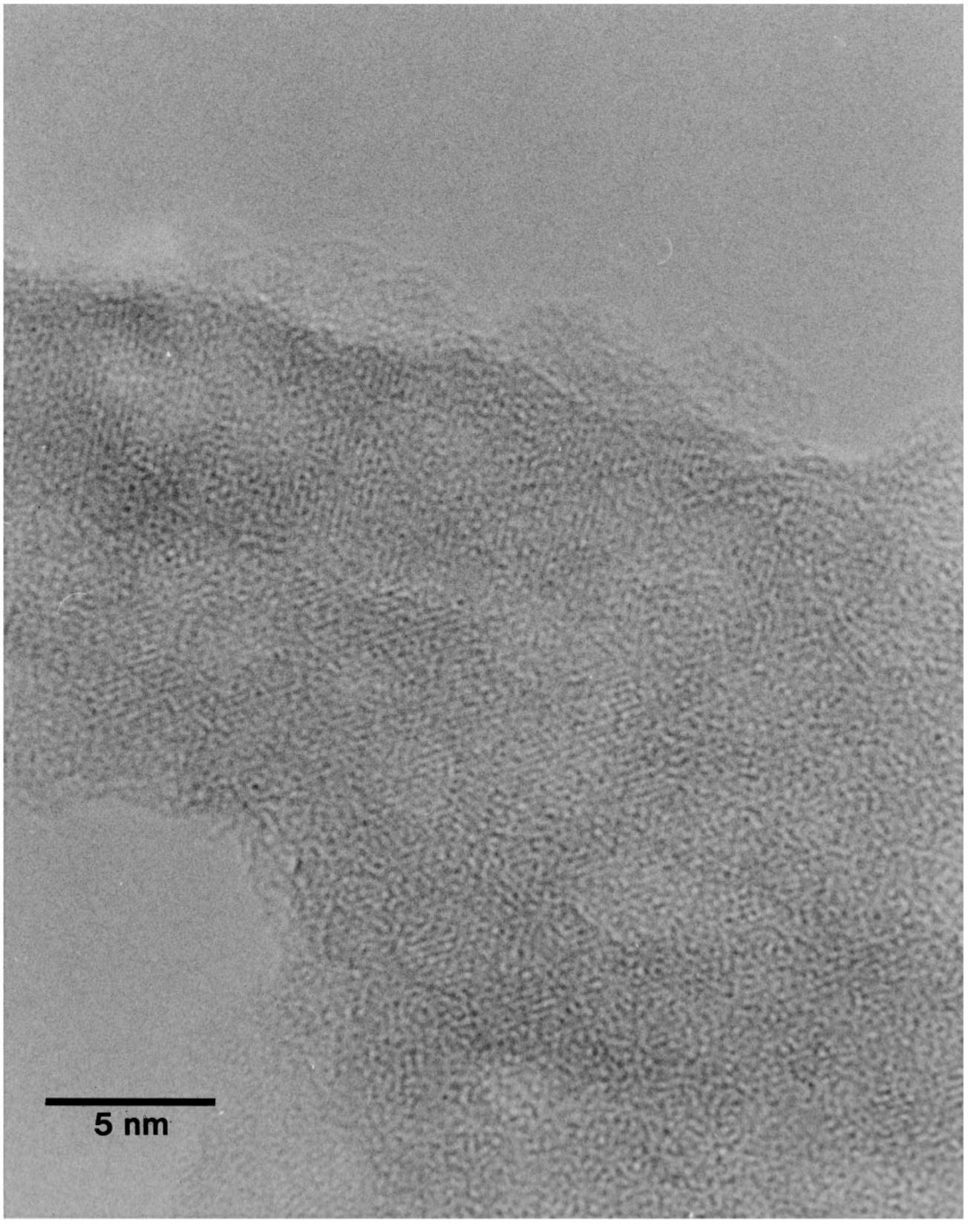

FIG. 2. TEM images of (a) Al_2O_3, (b) CeO_x/Al_2O_3, (c) 5 wt% $CeO_x/Pd/Al_2O_3$, and (d) 30 wt% $CeO_x/Pd/Al_2O_3$.

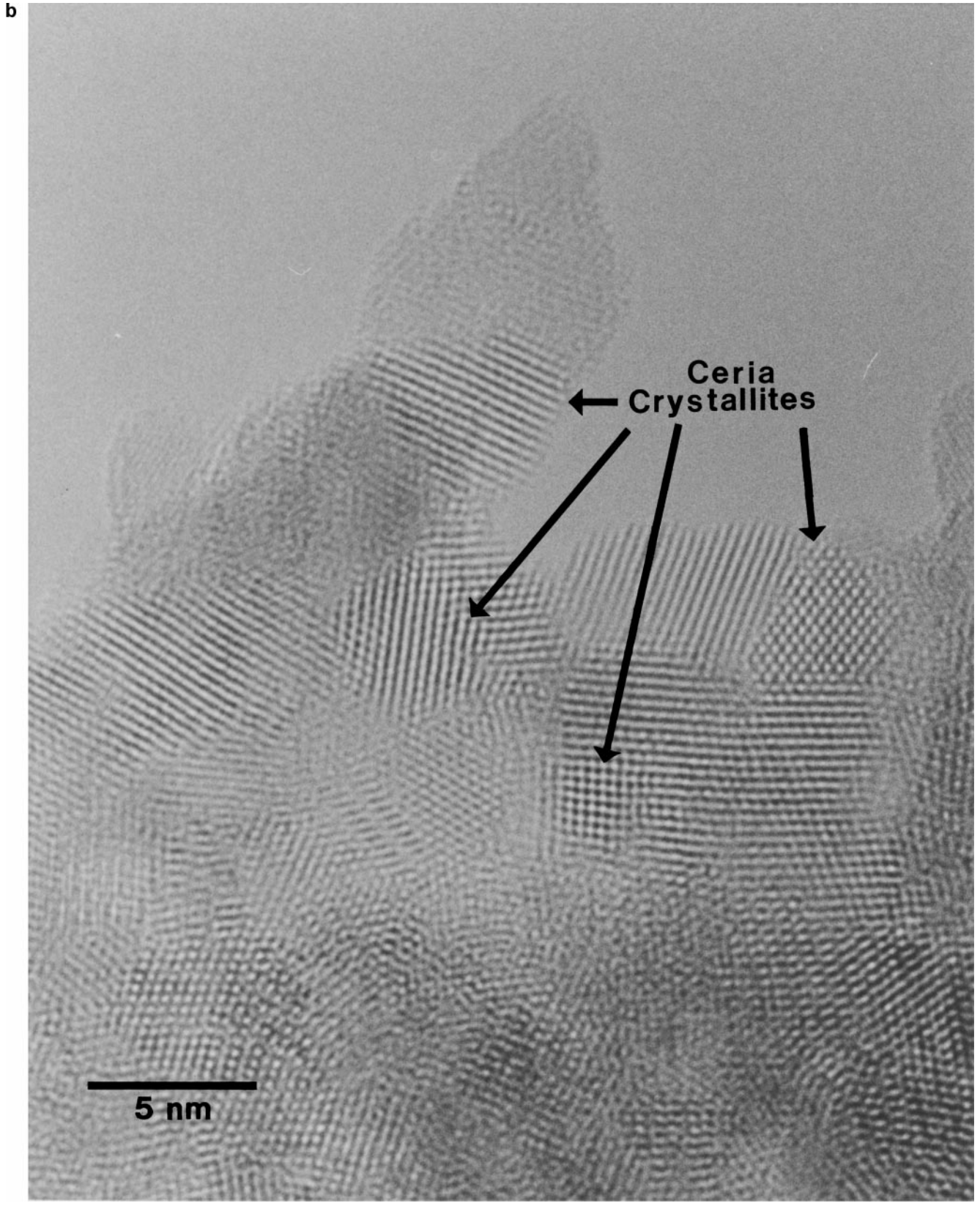

FIG. 2—*Continued*

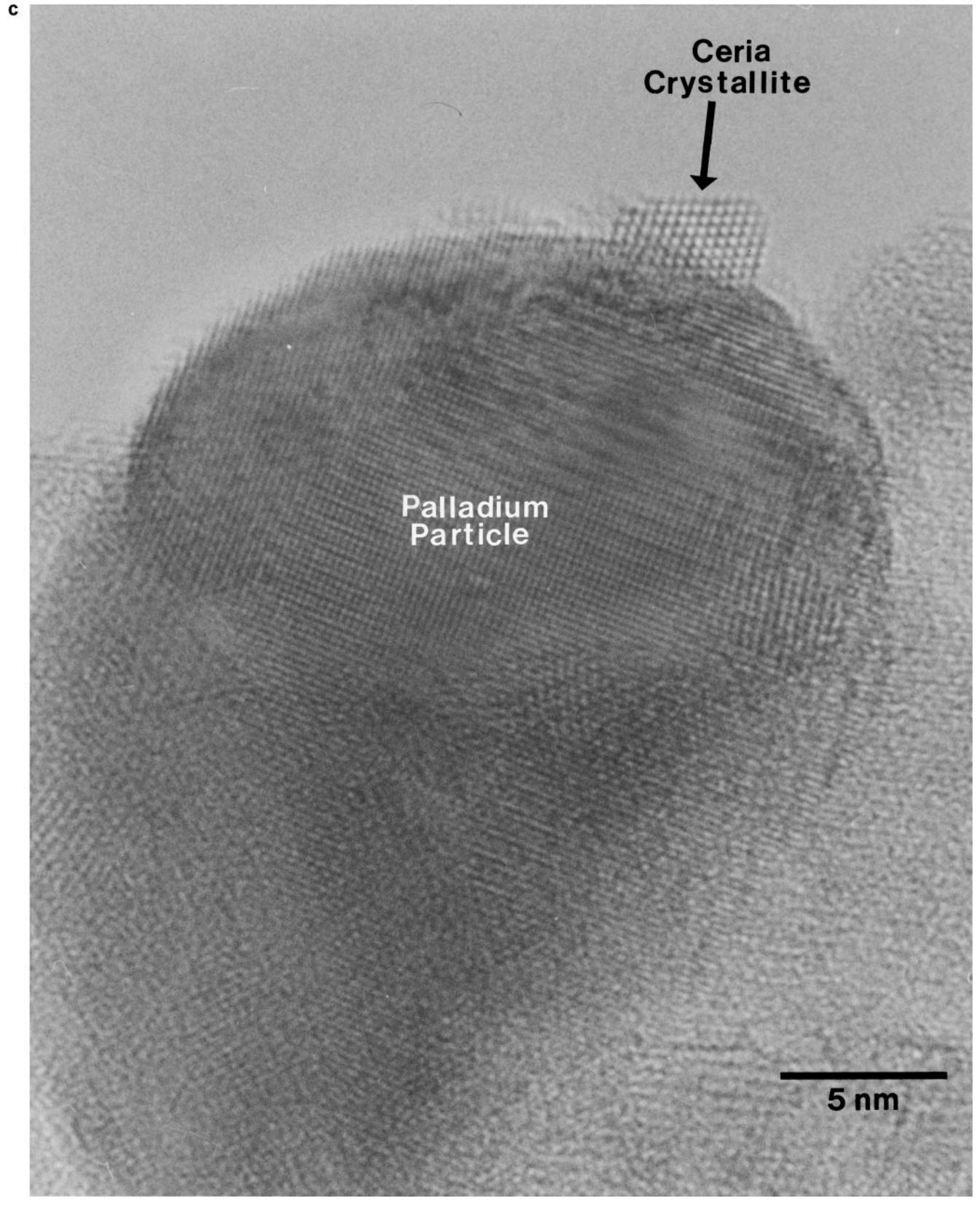

FIG. 2—*Continued*

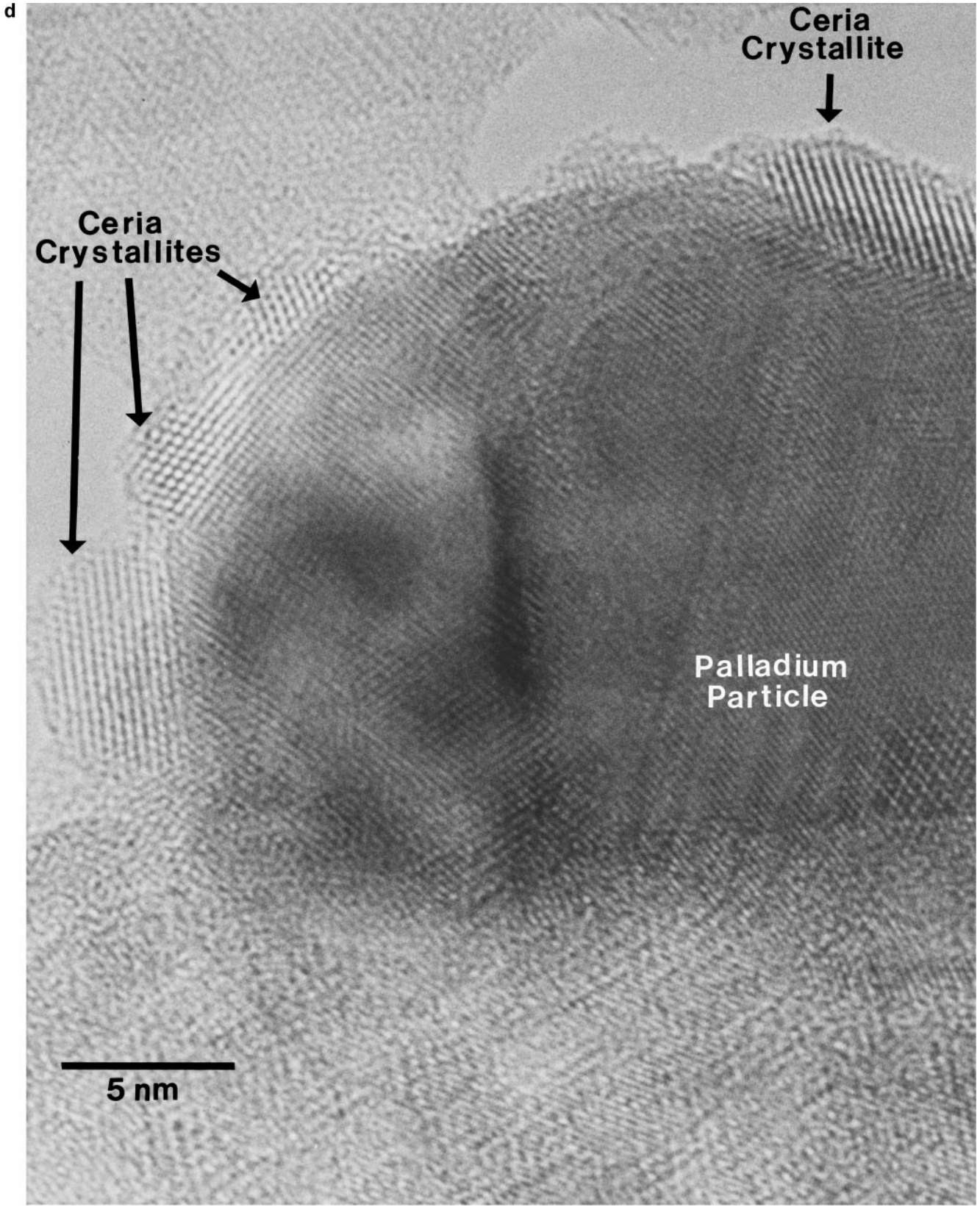

FIG. 2—*Continued*

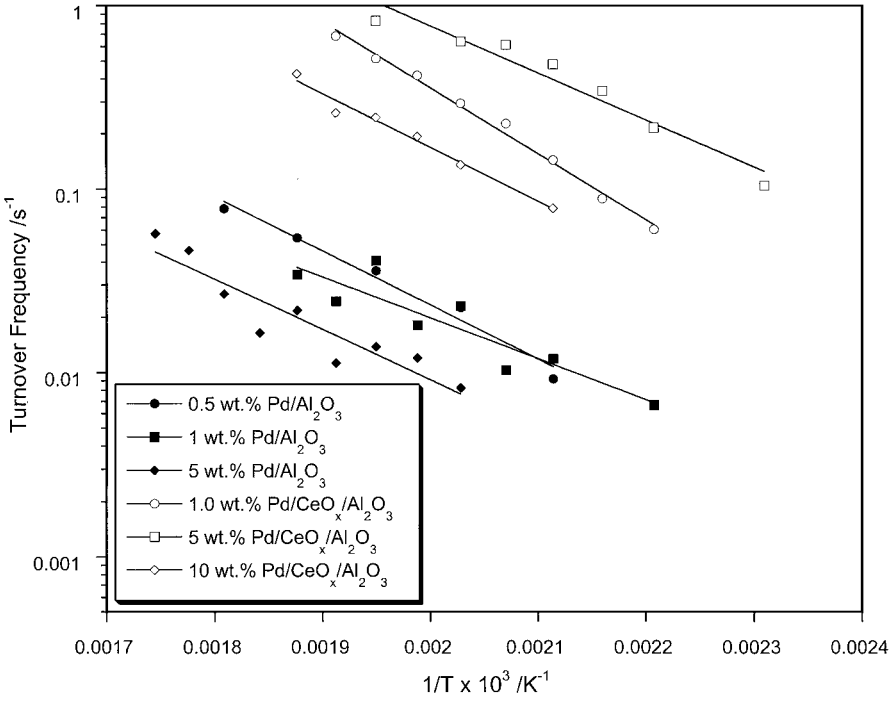

FIG. 3. Arrhenius-type plots for the NO + CO reaction over 5 wt% Pd/Al_2O_3, 1.0 wt% Pd/Al_2O_3, 0.5 wt% Pd/Al_2O_3, 10 wt% $Pd/CeO_x/Al_2O_3$, 5 wt% $Pd/CeO_x/Al_2O_3$, and 1.0 wt% $Pd/CeO_x/Al_2O_3$ for reactant mixtures of 5.07 kPa of each NO and CO.

For the NO + CO reaction, the only products observed were N_2, N_2O, and CO_2. No NO_2 was detected in any reaction run. Evaluation of the Weisz–Prater criterion indicated that no pore diffusion limitations existed. Conversions for these experiments ranged from 3 to 6%.

Figure 3 shows Arrhenius-type plots for the NO + CO reaction on the Pd/Al_2O_3 and $Pd/CeO_x/Al_2O_3$ catalysts as a function of particle size. Apparent activation energies derived from these plots are presented in Table 2. Clearly, the ceria-promoted Pd catalysts are much more active than any of the unpromoted catalysts. Figure 4 compares the dinitrogen selectivity for the Pd/Al_2O_3 and $Pd/CeO_x/Al_2O_3$ catalysts as a function of temperature. Dinitrogen selectivity is defined as the rate of N_2 production divided by the rate of N_2 and N_2O production. For all Pd particle sizes, the presence of ceria decreased the dinitrogen selectivity.

The influence of reactant partial pressures on the rate of the NO + CO reaction for Pd/Al_2O_3 catalysts as a function

TABLE 2

Apparent Activation Energies and Reaction Orders

Catalyst	Apparent activation energy (kJ mol^{-1})	Reaction order	
		NO	CO
0.5 wt% Pd/Al_2O_3	51.0	0.51	−0.49
1 wt% Pd/Al_2O_3	42.6	0.72	−0.51
5 wt% Pd/Al_2O_3	59.8	1.02	−1.11
1 wt% $Pd/CeO_x/Al_2O_3$	68.9	[a]	−0.50
5 wt% $Pd/CeO_x/Al_2O_3$	76.6	[a]	[a]
10 wt% $Pd/CeO_x/Al_2O_3$	56.2	[a]	[a]
5 wt% $CeO_x/Pd/Al_2O_3$	31.3	[a]	[a]
10 wt% $CeO_x/Pd/Al_2O_3$	43.0	1.3	−0.97
30 wt% $CeO_x/Pd/Al_2O_3$	37.1	0.67	−0.32

[a] Indicates a nonconstant reaction order. See figures for details.

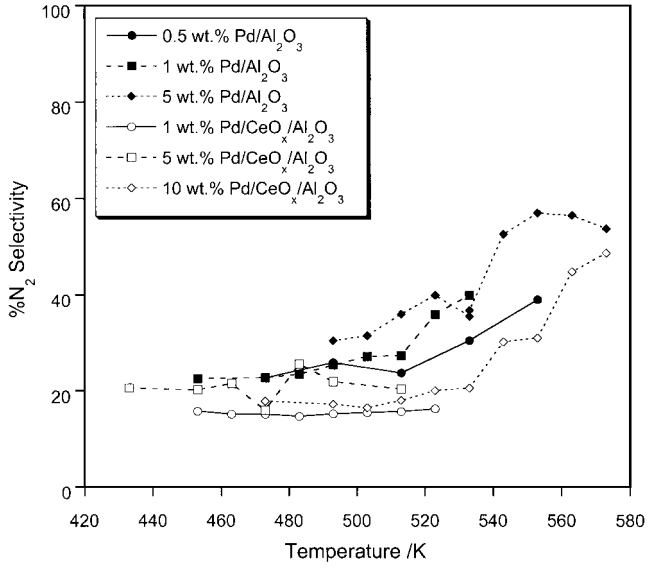

FIG. 4. N_2 selectivity vs temperature for the NO + CO reaction over 5 wt% Pd/Al_2O_3, 1.0 wt% Pd/Al_2O_3, 0.5 wt% Pd/Al_2O_3, 10 wt% $Pd/CeO_x/Al_2O_3$, 5 wt% $Pd/CeO_x/Al_2O_3$, and 1.0 wt% $Pd/CeO_x/Al_2O_3$.

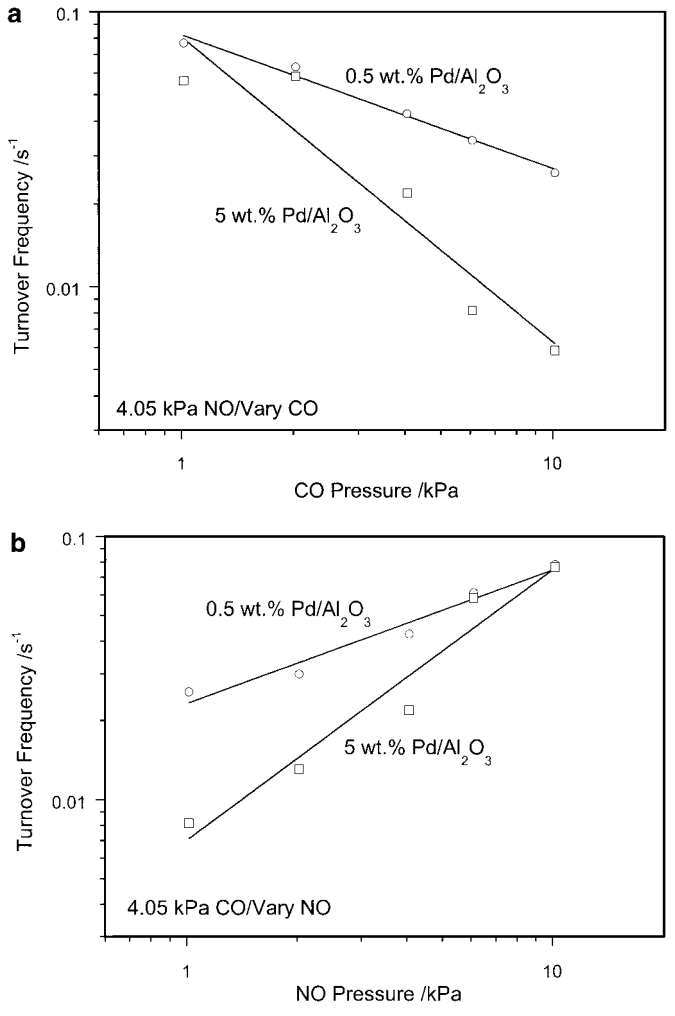

FIG. 5. Reaction order determination for the NO + CO reaction for 5 wt% Pd/Al_2O_3 and 0.5 wt% Pd/Al_2O_3. Figure 5a is for a fixed $P_{NO} =$ 4.05 kPa with a varying P_{CO}. Figure 5b is for a fixed $P_{CO} = 4.05$ kPa with a varying P_{NO}.

of particle size is summarized in Figs. 5a and 5b for CO and NO, respectively. The lines represent a linear regression of the rate data which yield orders for NO of 1.02 ± 0.15 for 5 wt% Pd/Al_2O_3 and 0.51 ± 0.15 for 0.5 wt% Pd/Al_2O_3 (based on NO consumption). The plot indicates the reaction order for CO becomes less negative and the reaction order for NO becomes less positive as the particle size decreases. Results for the other catalysts are shown in Table 2. Promotion of the Pd by ceria significantly altered the reaction orders. For instance, the NO reaction order was 1.02 on 5 wt% Pd/Al_2O_3 while for similar-sized Pd particles, the NO reaction order on 10 wt% $Pd/CeO_x/Al_2O_3$ was positive at low partial pressures of NO and became negative for high partial pressures of NO. Effects of CO and NO partial pressures on reaction rates as a function of particle size on the promoted catalysts are shown in Figs. 6a and 6b, respectively. For some catalysts, the reaction orders in both NO and CO were positive at low partial pressures and negative at high partial pressures, over the range of conditions investigated. The maximum in rate occurred near equimolar concentrations of NO and CO for these samples.

The Arrhenius-type plots for the catalysts with ceria deposited after palladium loading are shown in Fig. 7. Addition of 5 wt% ceria to the palladium results in an activity increase of approximately 1 order of magnitude. The subsequent addition of up to 30 wt% ceria results in only a marginal increase in activity. For comparison with the samples with palladium added on top of ceria, the turnover frequency for the 10 wt% $CeO_x/Pd/Al_2O_3$ is almost identical to that of the 1 wt% $Pd/CeO_x/Al_2O_3$ sample. Apparent activation energy and reaction orders for the $CeO_x/Pd/Al_2O_3$ samples are also given in Table 2. Apparent activation energies were all similar at about 37 kJ mol^{-1} and, compared to the unpromoted 1 wt% Pd/Al_2O_3 sample, the addition of ceria had very little effect on the apparent

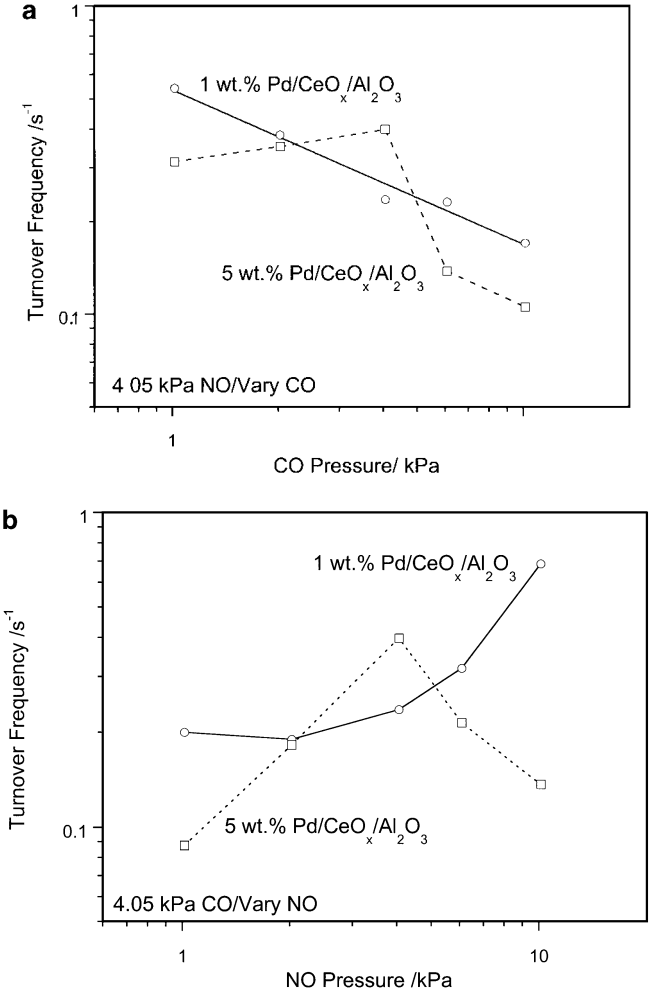

FIG. 6. Reaction order determination for the NO + CO reaction for 5 wt% $Pd/CeO_x/Al_2O_3$ and 1.0 wt% $Pd/CeO_x/Al_2O_3$. Figure 6a is for a fixed $P_{NO} = 4.05$ kPa with a varying P_{CO}. Figure 6b is for a fixed $P_{CO} = 4.05$ kPa with a varying P_{NO}.

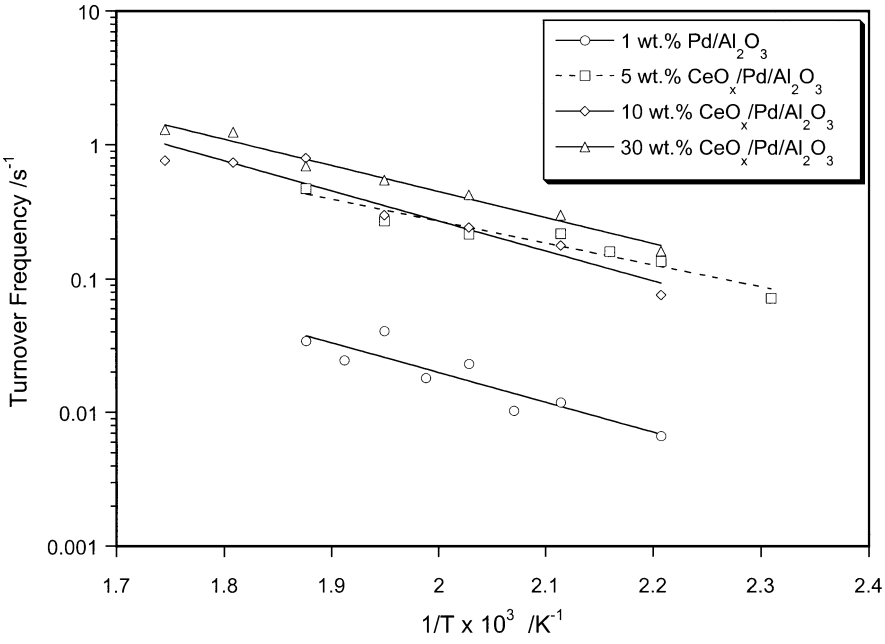

FIG. 7. Arrhenius-type plots for the NO + CO reaction over 1.0 wt% Pd/Al_2O_3, 5 wt% $CeO_x/Pd/Al_2O_3$, 10 wt% $CeO_x/Pd/Al_2O_3$, and 30 wt% $CeO_x/Pd/Al_2O_3$ for reactant mixtures of 5.07 kPa of each NO and CO.

activation energy. Ceria did affect the NO and CO reaction orders, however. The activity of a catalyst with 5 wt% ceria exhibited a maximum with respect to reactant partial pressure, which is similar to the behavior of several $Pd/CeO_x/Al_2O_3$ samples. Catalysts with higher ceria loadings exhibited constant reaction orders for NO and CO over the range of conditions tested.

The effect of Pd particle size on the adsorption of NO and subsequent TPD is shown in Fig. 8. The signal for NO is not shown since it was very large and similar for all catalysts. For the smallest Pd particles (1.1 nm), the major desorption feature is attributed to O_2 which desorbed with a peak temperature of 720 K. Dinitrogen desorbed in a very broad peak at ~550 K and a smaller peak at 700 K. A small amount of N_2O also desorbed with a peak at 700 K. For slightly larger particles (1.5 nm), the main feature was also an O_2 desorption peak at 710 K. For the largest Pd particles (4.5 nm), the O_2 desorption feature was no longer present. Instead, the major desorption product was N_2O with two broad desorption peaks at 430 and 610 K. Therefore, the effect of increasing the Pd particle size from 1 to 5 nm appears to be the suppression of O_2 desorption and enhancement of N_2O desorption.

The TPD plots in Fig. 9 show the effect of depositing ceria on top of supported palladium. For 1 wt% Pd/Al_2O_3 (1.5-nm Pd particles), the major desorption feature at 710 K was again due to O_2. However, addition of 5 wt% ceria to this sample suppressed the O_2 desorption peak. A broad N_2O desorption peak at 675 K and a second smaller peak at 440 K were observed instead. Incorporation of additional 25 wt% ceria resulted in the reappearance of an O_2 desorption feature and a decrease in the magnitude of the N_2O peak, which shifted to a slightly higher temperature. For 10 wt% CeO_x/Al_2O_3 with no Pd present, there was a large O_2 desorption peak at 710 K with N_2 and N_2O desorption similar to that of the previous sample. Apparently, the effect of ceria addition after loading of Pd particles results in suppression of the O_2 peak and the increase of the N_2O peak as the ceria loading increases. High loadings of ceria result in a new O_2 desorption feature due to the ceria crystallites.

Figure 10 shows the TPD plots for various sizes of Pd particles deposited onto CeO_x/Al_2O_3. The major feature for the smallest particles (<1 nm) was a large O_2 peak at 710 K. Other features include two broad N_2 desorption peaks at 450 and 700 K and an N_2O desorption peak at 700 K. Increasing the Pd particle size to 2.0 nm suppressed the O_2 peak while increasing the magnitude of the N_2 and N_2O peaks, which were also shifted to lower temperatures of 670 and 620 K, respectively. For the largest ceria-promoted Pd particles (9 nm), two well-defined N_2 and N_2O desorption peaks were observed at temperatures of 620 and 590 K, respectively. The overall effect of Pd particle size for the $Pd/CeO_x/Al_2O_3$ samples was to suppress O_2 formation while enhancing N_2 and N_2O formation.

DISCUSSION

The TEM images clearly show that ceria typically forms small, well-dispersed crystallites on the alumina support.

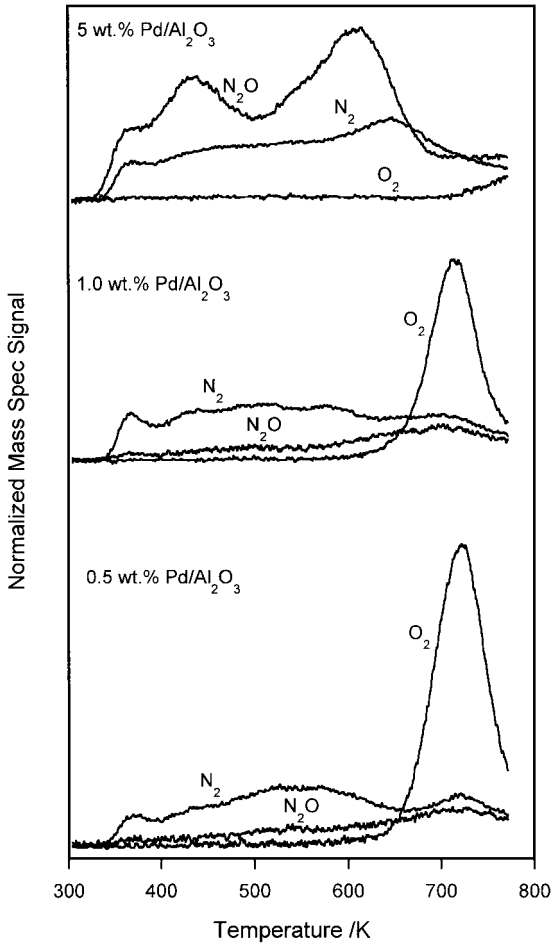

FIG. 8. TPD curves for N_2, O_2, and N_2O desorption following a saturation exposure to NO for 0.5 wt% Pd/Al_2O_3, 1.0 wt% Pd/Al_2O_3, and 5 wt% Pd/Al_2O_3.

For the samples with ceria added after Pd incorporation, ceria was seen to deposit as small crystallites on top of and/or near the Pd particles. It does not appear that ceria formed a very thin film that covers the particle. As the amount of postdeposited ceria increased, the number of ceria crystallites in contact with the Pd particles increased. Although the Pd particles shown in these TEM images are larger than the average particle size determined by chemisorption, they serve to illustrate that ceria crystallites were observed near the metal particles. For the samples with Pd deposited after ceria, the Pd was still found to be in contact with small ceria crystallites. However, we did not find any evidence for ceria migration on top of the Pd particles.

The NO + CO reaction over single-crystal Pd has been shown to be structure-sensitive (2, 9). The Pd(111) surface was observed to be more active than the Pd(100) surface which is in turn more active than the Pd(110) surface. The activity results contrast with the observation that the Pd(100) surface is more active than the Pd(111) surface for NO dissociation (2, 9). Therefore, removal of a thermally stable atomic nitrogen species (N_a) is thought to be more important than NO dissociation in determining the kinetics of this reaction under some conditions. This conclusion is also indicated by previous NO TPD studies that have shown the less active Pd(100) surface is 80% covered by N atoms while the more active Pd(111) surface is only 20% covered. This concept can be used to explain the particle size effect for unpromoted and ceria-promoted Pd.

To understand the role of Pd particle size on ceria-promoted Pd for the NO + CO reaction, it is desirable to first study the effect of Pd particle size on unpromoted Pd. Previous results by Rainer *et al.* have demonstrated that activity for the NO + CO reaction decreases as the Pd particle size decreases from 120 to 6.0 nm (2). The specific activity of our 5 wt% Pd/Al_2O_3 (4.5-nm Pd particles) was only slightly higher than the activity reported by Rainer *et al.* for a catalyst with 6.0-nm Pd particles. However, as we decreased Pd particle size to 1.5 nm or smaller, we observed a threefold increase in turnover frequency. Rainer *et al.* reported an increase of activity of 50% as the Pd particle size was decreased from 6 to <3 nm, but this observation was not discussed.

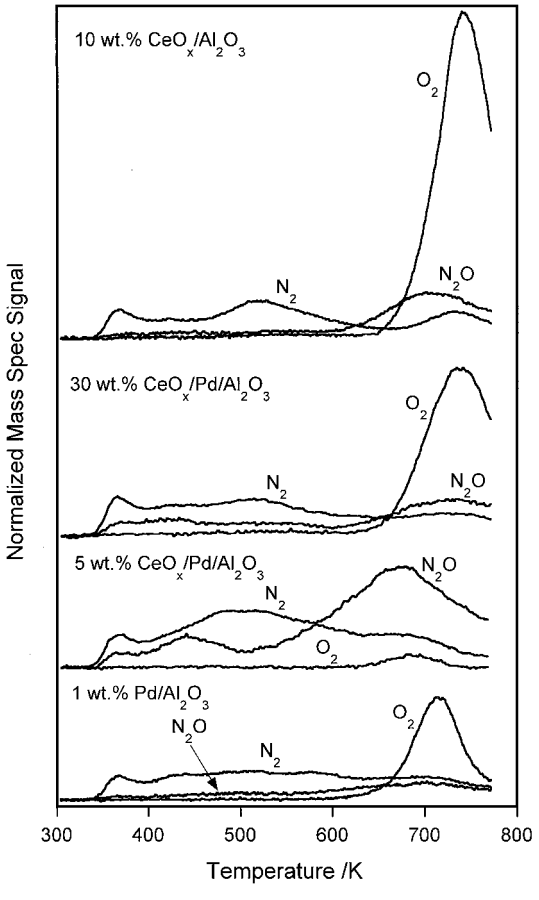

FIG. 9. TPD curves for N_2, O_2, and N_2O desorption following a saturation exposure to NO for 1.0 wt% Pd/Al_2O_3, 5 wt% $CeO_x/Pd/Al_2O_3$, 30 wt% $CeO_x/Pd/Al_2O_3$, and 10 wt% CeO_x/Al_2O_3.

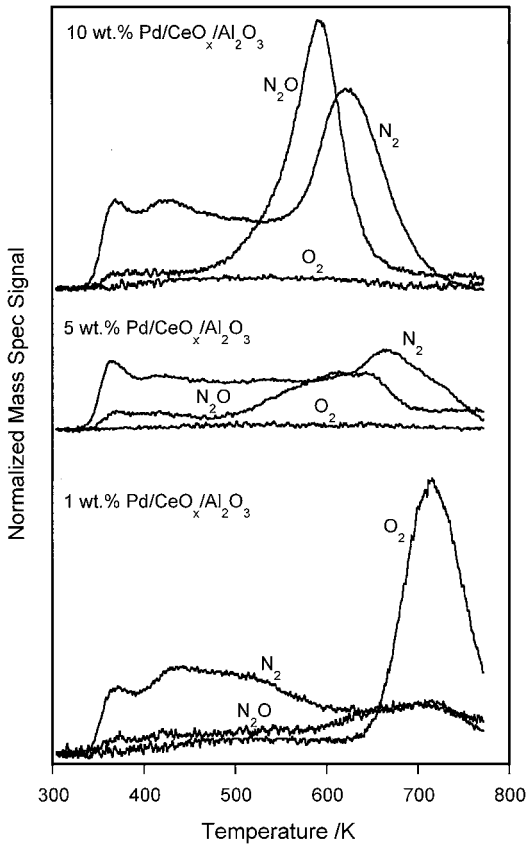

FIG. 10. TPD curves for N_2, O_2, and N_2O desorption following a saturation exposure to NO for 1.0 wt% $Pd/CeO_x/Al_2O_3$, 5 wt% $Pd/CeO_x/Al_2O_3$, and 10 wt% $Pd/CeO_x/Al_2O_3$.

The measured NO and CO reaction orders as a function of Pd particle size help to provide an understanding of this increase in activity for the smallest particles. In an earlier paper, a reaction rate expression was developed for the NO + CO reaction over Rh and Pd in which the NO reaction order can be positive, zero, or negative, depending on the relative surface coverages of NO, CO, and N atoms (6). High coverage of NO results in a negative NO reaction order, high coverage of CO results in a positive NO reaction order, and high coverage of N atoms results in zero reaction orders for both NO and CO. For the 5 wt% Pd/Al_2O_3 sample, a NO reaction order of 1.02 indicates high CO coverage (and correspondingly low coverages of NO and N). However, as the particle size decreased, the NO reaction order decreased. This implies that the surface coverage of N atoms increases as the particle size decreases. Enhanced NO dissociation and/or N atom stabilization can account for this change in reaction order. Since the catalytic activity increased while the NO reaction order decreased (indicating higher N atom coverage), we believe that enhanced NO dissociation is more likely. The ability of small Pd particles to enhance dissociation of adsorbed molecules has also been observed in other systems. Ichikawa *et al.* showed that small particles of Pd (<2 nm) can disproportionate CO to carbon and CO_2 whereas larger particles cannot (14). This disproportionation ability was attributed to small particles preferring icosahedral packing instead of the standard face-centered cubic structure (15). We suggest that the observed increase in NO + CO activity for small particles results from the enhanced ability to dissociate NO, similar to the case described above for CO dissociation.

It is also instructive to discuss our results in light of those for Rh, a typical NO_x reduction catalyst. The activity for the NO + CO reaction over supported Rh reportedly decreases as Rh particle size decreases from 70 to <1 nm (16). An increase in activity was not observed for very small Rh particles, which is in contrast to our observation with supported Pd. This is not surprising in light of the ability of Rh to readily dissociate NO (17, 18). In addition, under identical experimental conditions for NO + CO, the observed reaction orders on Rh/Al_2O_3 imply a high N atom coverage whereas the orders on Pd/Al_2O_3 (4.5 nm) suggest a low N atom coverage (6). Finally, very small Rh particles are not required to dissociate CO (19).

In addition to Pd particle size, ceria plays a crucial role in the NO + CO reaction. The turnover frequency for the ceria-promoted 5 wt% Pd was approximately 2 orders of magnitude greater than that for the unpromoted 5 wt% Pd. Although alumina-supported ceria catalyzed the NO + CO reaction with no metal present, the reaction rate, on a per gram basis, was a factor of 4 lower than any other catalyst studied in this work. Therefore, the enhancement in observed rates is either due to a modification of the metal particles or creation of new sites at the metal/promoter interface. To explain the enhanced activity for ceria-promoted Rh, Oh proposed that NO dissociates at interface sites (7). Based on our observations of the kinetics of unpromoted and ceria-promoted Pd, we have extended this explanation to include Pd (6). The enhancement of NO dissociation at the metal–promoter interface can also be used to explain the effect of Pd particle size on catalysis by ceria-promoted Pd.

For the sample with the largest Pd particles (10 wt% $Pd/CeO_x/Al_2O_3$), which should have the smallest interfacial contact relative to metal particle surface area, the observed promotional effect was the smallest. In this case, the enhanced NO dissociation provided by the promoter interface did not affect surface coverages of adsorbed intermediates until intermediate NO pressures were attained, as indicated by the NO reaction order. At intermediate NO pressures, the coverage of N atom was high and the reaction appeared to be zero order in NO. The promotional role of the Pd/ceria interface is evidently diminished for very large particles. For the 5 wt% $Pd/CeO_x/Al_2O_3$ sample with the highest catalytic activity, the proportion of promoter/metal interface to Pd surface area was greater, thus providing more dissociated N atoms to the Pd metal surface. However, as the Pd particles were made smaller, the amount of open surface facets increased, which resulted

in a partial stabilization and higher fractional surface coverage of N atoms. The high observed promotional effect of ceria on this sample indicates a balance between the interfacial contact with promoter and the stabilization of N atoms at the surface. This balance is between the ability of the interface to provide N atoms through increased NO dissociation at the Pd–ceria interface and the ability of the metal particle to react the N atoms off the surface. For the smallest particles, the ability of open facets to stabilize adsorbed N atoms overcomes the ability of the interface to enhance dissociation. The high fractional coverage of N atoms then results in decreased activity, as observed for single crystals. A high coverage of N atoms results in a NO reaction order of zero, even for low P_{NO} on the smallest particles.

Apparent activation energies for the unpromoted catalysts were similar at around 50 kJ/mol and there was no obvious influence of particle size. For the ceria-promoted samples, the apparent activation energies were slightly higher, ranging from 56.2 to 76.6 kJ/mol. The apparent activation energy for the least promoted sample was similar to that for the unpromoted samples. Dinitrogen selectivity was typically lower for the ceria-promoted than for the unpromoted samples. The temperature appears to have a larger effect on selectivity than presence of the promoter. At a temperature of 520 K, the selectivity was highest for the smallest unpromoted particles and lowest for the largest unpromoted particles. This result is consistent with those of Rainer *et al.* who reported that the more open single-crystal faces had higher N_2 selectivities than the close-packed surfaces (2). For the ceria-promoted samples, the most active sample had the highest selectivity while the less active samples had lower selectivity. The lower selectivity for the ceria-promoted samples is not easily interpreted in light of the expected increase in NO dissociation for these samples which should result in greater N_2 production due to the presence of additional N atoms. This inconsistency was also observed by Rainer *et al.* for Pd/Al_2O_3 catalysts (2) and Oh and Eickel for Rh/Al_2O_3 catalysts (16). Perhaps ceria also affects product formation. It is important to note that although selectivity decreased slightly, the activity for both N_2 and N_2O formation increased significantly with ceria promotion.

In an attempt to separate the effects of the Pd/ceria interface and Pd particle size, we prepared a series of samples with constant particle size and increased the Pd/ceria interface by depositing ceria on top of the Pd. The rate measurements showed that the addition of only 5 wt% ceria to 1 wt% Pd/Al_2O_3 provided an order of magnitude increase in activity. The rate on the 10 wt% ceria sample was essentially the same. The activities of 1 wt% $Pd/CeO_x/Al_2O_3$ and 10 wt% $CeO_x/Pd/Al_2O_3$ were similar, indicating that the order of ceria addition is not a major factor in the catalyst preparation method. The presence of additional ceria up to 30 wt% total resulted in only a slight increase in activity. Dinitrogen selectivities for all ceria-containing samples were similar.

The large increase in rate accomplished by adding 5 wt% ceria indicated that submonolayer coverages of ceria can affect activity. The fact that the rate did not increase significantly as additional ceria was added may indicate preferential formation of ceria crystallites near the Pd particles during the calcination process. In addition to activity, the effect of increasing the Pd/ceria interfacial contact can be seen in the reaction orders. Incorporation of 5 wt% ceria changed the NO reaction order from the constant 1.02 for 1 wt% Pd/Al_2O_3 to a variable reaction order with a maximum similar to the 5 and 10 wt% $Pd/CeO_x/Al_2O_3$ samples. Again, this type of reaction order behavior indicates that NO dissociation is enhanced at intermediate pressures. For the 10 wt% ceria sample the constant reaction order indicates that even at intermediate to high P_{NO}, the additional Pd/ceria interface is dissociating NO rapidly enough to prevent inhibition by NO. Finally, at 30 wt% ceria, the increased Pd/ceria interface dissociates NO rapidly enough to build up N atoms on the Pd metal and alter the NO and CO reaction orders appropriately.

The results from TPD of preadsorbed NO substantiate the conclusions derived from kinetic analysis. Indeed, the desorption of products was significantly affected by Pd particle size. For unpromoted Pd, the smallest Pd particles (<1.5 nm) were able to desorb dioxygen whereas desorption peaks for N_2 and N_2O were very broad and small. However, for the largest Pd particles (4.5 nm), no O_2 desorption was observed and instead the oxygen was desorbed in the form of N_2O product. Since enhanced NO dissociation can lead to O_2 desorption, and less NO dissociation can lead to N_2O desorption, the TPD results provide additional evidence for the enhanced dissociation of NO on small Pd particles. Desorption of O_2 from Pd particles during NO TPD was not previously observed by Xu and Goodman or Cordatos *et al.*; however, they did not have particles smaller than 1.6 nm (11, 20). The O_2 desorption peak for very small particles may suggest the predominant facet that is exposed. For example, some authors did not observe O_2 desorption during TPD from single-crystal Pd(111) previously exposed to NO (18, 21). Others report that chemisorbed O_2 desorbs from Pd(111) at temperatures greater than about 800 K (22, 23), which exceeds the maximum temperature in our work. Dioxygen desorbing from the more open Pd(110) surface gives two desorption peaks at about 700 and 800 K, with the low-temperature peak originating from subsurface oxygen (24–26). Desorption of subsurface oxygen prepared by decomposition of NO_2 on Pd(111) generates lower temperature O_2 TPD features (27), which are consistent with O_2 desorption from the more open Pd(110) crystal face previously exposed to O_2. Apparently, open-crystal planes of Pd facilitate incorporation of subsurface oxygen. Thus, the observation of O_2 desorption from small Pd particles reported here indicates that they likely expose open-faceted surfaces which may lead to subsurface oxide formation. Our TPD results for N_2 and N_2O as a function of particle size are

qualitatively similar to those of Cordatos *et al.* and Xu and Goodman since the smallest particles evolved mostly N_2 and very little N_2O and the larger particles produced more N_2O and less N_2 (11, 20). Enhanced NO dissociation on the smaller particles is also consistent with N_2 being the predominant N-containing product evolved during TPD from small particles whereas N_2O is preferred on large particles.

Addition of ceria on top of supported Pd particles suppressed O_2 desorption at low ceria loading. In addition, a low-temperature N_2 peak appeared, indicating enhanced NO dissociation. Higher loadings of ceria resulted in the reappearance of a large O_2 desorption feature at ~700 K. Since O_2 evolution was detected from supported ceria (without Pd present) during TPD of adsorbed NO, we attribute the reappearance of an O_2 feature on high ceria-loaded Pd/Al_2O_3 to the ceria component.

For the samples with ceria deposited prior to the Pd, O_2 desorption was only observed from the sample with the smallest Pd particles. Enhanced NO dissociation on this sample was indicated by the preferential desorption of N_2 instead of N_2O. As the Pd particle size increased, the O_2 desorption was completely suppressed. For the largest particles, both N_2O and N_2 desorption features became well defined, similar to features seen in single-crystal studies. Indeed, the N_2O and N_2 peak temperatures are close to the single-crystal values of ~510 K for N_2O and 650 K for N_2 reported by Schmick and Wassmuth and 480 and 670 K by Conrad *et al.* for a Pd(111) surface (18, 28). The N_2O and N_2 peak temperatures for the sample with the largest Pd particles are also similar to the results obtained by Rainer *et al.* for 8 nm, unpromoted Pd/Al_2O_3 particles (525 and 600 K, respectively) (2). The agreement between the TPD of NO from promoted, large Pd particles and the Pd single-crystal studies illustrates that the Pd/ceria interface does not significantly affect the results over the largest Pd particles in this study. When comparing the promotional effect of ceria on TPD, the enhanced NO dissociation provided by the Pd/ceria interface served to increase the amount of N_2 desorbed at lower temperatures. Similar increased N_2 desorption was observed by Cordatos and Gorte for Pd particles on flat polycrystalline ceria supports (29).

CONCLUSIONS

Palladium particles of 1-nm average diameter were more active than 4.5-nm Pd particles for the NO + CO reaction. Results from kinetic studies and TPD of NO suggest that NO dissociation is enhanced on the smallest particles, but that N atoms are also held more strongly on the Pd. When ceria is used to promote the Pd, the activity for NO + CO was a maximum for 2-nm-sized Pd particles. A maximum in activity results from the balance between the Pd/ceria interface that enhances NO dissociation and the close-packed planes of the Pd particle surface that facilitate product formation and/or desorption. The variations in apparent reaction orders and results from TPD were consistent with the idea that NO dissociation is promoted on very small particles (1 nm) and by addition of ceria.

Characterization of the catalysts by TEM indicated that ceria was typically in the form of small crystallites from 3 to 7 nm in diameter. For the samples with ceria deposited after Pd, the ceria crystallites were typically deposited near or on top of the Pd particle. No evidence of a ceria thin film on the Pd was detected.

ACKNOWLEDGMENT

This work was supported by the Division of Chemical Sciences, Office of Basic Energy Sciences, Office of Energy Research, U.S. Department of Energy.

REFERENCES

1. Taylor, K. C., *Catal. Rev.-Sci. Eng.* **35**, 457 (1993).
2. Rainer, D. R., Vesecky, S. M., Koranne, M., Oh, W. S., and Goodman, D. W., *J. Catal.* **167**, 234 (1997).
3. Rainer, D. R., Koranne, M., Vesecky, S. M., and Goodman, D. W., *J. Phys. Chem. B* **101**, 10769 (1997).
4. Almusaiteer, K., and Chuang, S. S. C., *J. Catal.* **180**, 161 (1998).
5. Almusaiteer, K., and Chuang, S. S. C., *J. Catal.* **184**, 189 (1999).
6. Holles, J. H., Switzer, M. S., and Davis, R. J., *J. Catal.* **190**, 247 (2000).
7. Oh, S. H., *J. Catal.* **124**, 477 (1990).
8. Le Normand, F., Hilaire, L., Kili, K., Krill, G., and Maire, G., *J. Phys. Chem.* **92**, 2561 (1988).
9. Vesecky, S. M., Chen, P., Xu, X., and Goodman, D. W., *J. Vac. Sci. Technol. A* **13**, 1539 (1995).
10. Vesecky, S. M., Rainer, D. R., and Goodman, D. W., *J. Vac. Sci. Technol. A* **14**, 1457 (1996).
11. Xu, X., and Goodman, D. W., *Catal. Lett.* **24**, 31 (1994).
12. Benson, J. E., Hwang, H. S., and Boudart, M., *J. Catal.* **30**, 146 (1973).
13. Boudart, M., and Djéga-Mariadassou, G., "Kinetics of Heterogeneous Catalytic Reactions." Princeton Univ. Press, Princeton, NJ, 1984.
14. Ichikawa, S., Poppa, H., and Boudart, M., *J. Catal.* **91**, 1 (1985).
15. Poppa, H., Moorhead, R. D., and Avalos-Borja, M., *J. Vac. Sci. Technol. A* **7**, 2882 (1989).
16. Oh, S. E., and Eickel, C. C., *J. Catal.* **128**, 526 (1991).
17. Belton, D. N., DiMaggio, C. L., Schmieg, S. J., and Ng, K. Y. S., *J. Catal.* **157**, 559 (1995).
18. Schmick, H.-D., and Wassmuth, H.-W., *Surf. Sci.* **123**, 471 (1982).
19. Solymosi, F., and Erdöhelyi, A., *Surf. Sci.* **110**, L630 (1981).
20. Cordatos, H., Bunluesin, T., and Gorte, R. J., *Surf. Sci.* **323**, 219 (1995).
21. Davies, P. W., and Lambert, R. M., *Surf. Sci.* **110**, 227 (1981).
22. Conrad, H., Ertl, G., Kuppers, J., and Latta, E. E., *Surf. Sci.* **65**, 245 (1977).
23. Guo, X., Hoffman, A., and Yates, J. T., Jr., *J. Chem. Phys.* **90**, 5787 (1989).
24. He, J.-W., Memmert, U., and Norton, P. R., *J. Chem. Phys.* **90**, 5088 (1989).
25. Milun, M., Pervan, P., Vajic, M., and Wandelt, K., *Surf. Sci.* **211/212**, 887 (1989).
26. Bondzie, V. A., Kleban, P., and Dwyer, D. J., *Surf. Sci.* **347**, 319 (1996).
27. Banse, B. A., and Koel, B. E., *Surf. Sci.* **232**, 275 (232).
28. Conrad, H., Ertl, G., Kuppers, J., and Latta, E. E., *Surf. Sci.* **65**, 235 (1977).
29. Cordatos, H., and Gorte, R. J., *J. Catal.* **159**, 112 (1996).